NANO · MICRO small
www.small-journal.com

Nanotube-Like Electronic States in [5,5]-C_{90} Fullertube Molecules.

Óscar Jover, Alberto Martín-Jiménez, Hannah M. Franklin, Ryan M. Koenig, José I. Martínez, Nazario Martín, Koen Lauwaet, Rodolfo Miranda, José M. Gallego, Steven Stevenson, and Roberto Otero**

Fullertubes, that is, fullerenes consisting of a carbon nanotube moiety capped by hemifullerene ends, are emerging carbon nanomaterials whose properties show both fullerene and carbon nanotube (CNT) traits. Albeit it may be expected that their electronic states show a certain resemblance to those of the extended nanotube, such a correlation has not yet been found or described. Here it shows a scanning tunneling microscopy (STM) and spectroscopy (STS) characterization of the adsorption, self-assembly, and electronic structure of 2D arrays of [5,5]-C_{90} fullertube molecules on two different noble metal surfaces, Ag(111) and Au(111). The results demonstrate that the shape of the molecular orbitals of the adsorbed fullertubes corresponds closely to those expected for isolated species on the grounds of density functional theory calculations. Moreover, a comparison between the electronic density profiles in the bands of the extended [5,5]-CNT and in the molecules reveals that some of the frontier orbitals of the fullertube molecules can be described as the result of the quantum confinement imposed by the hemifullerene caps to the delocalized band states in the extended CNT. The results thus provide a conceptual framework for the rational design of custom fullertube molecules and can potentially become a cornerstone in the understanding of these new carbon nanoforms.

1. Introduction

Fullertubes[1–3] are the last incorporation to the growing family of carbon nanoforms, whose members (fullerenes, CNTs, graphene, and nanographenes) have so prominently contributed to the development of modern Nanoscience and Nanotechnology.[4] Fullertubes consist of a central CNT region capped by two hemifullerene moieties at both ends[1,3] and, as such, can be expected to show intermediate properties between CNTs and fullerenes. Many of the exciting properties of carbon nanoforms arise from their peculiar electronic structure, enabling ballistic transport in CNTs,[5] strong electron-accepting behavior in fullerenes,[6–9] the existence of massless fermions as quasiparticles in graphene[10] or the magnetic properties of certain type of edges in graphene nanostructures.[11,12] From this point of view, the characterization of the energies and wave-functions of fullertubes is an essential step towards realizing their potential and clarifying their field of application.

Moreover, given the recent experimental discoveries of new molecules of pristine [5,5] C_{100} in 2020[3] and [5,5] C_{120} fullertubes in 2022,[2] a question naturally arises: Is the fullertube chemical and electronic behavior governed predominantly by their fullerene or CNT moieties? Furthermore, as the fullertube length increases from [5,5] C_{90} to [5,5] C_{100} to [5,5] C_{120} and beyond, at what tubular length would the properties of

Ó. Jover, R. Miranda, R. Otero
Dep. De Física de la Materia Condensada
Universidad Autónoma de Madrid
Madrid 28049, Spain
E-mail: roberto.otero@uam.es

Ó. Jover, A. Martín-Jiménez, N. Martín, K. Lauwaet, R. Miranda, R. Otero
IMDEA Nanoscience
Madrid 28049, Spain

The ORCID identification number(s) for the author(s) of this article can be found under https://doi.org/10.1002/smll.202307611

DOI: 10.1002/smll.202307611

H. M. Franklin, R. M. Koenig, S. Stevenson
Dep. Of Chemistry and Biochemistry
Purdue University Fort Wayne
Fort Wayne, IN 46805, USA
E-mail: stevenss@pfw.edu

J. I. Martínez, J. M. Gallego
Instituto de Ciencia de Materiales (ICMM)
CSIC
Madrid 28049, Spain

N. Martín
Dep. De Química OrgánicaFacultad de Ciencias Químicas
Universidad Complutense de Madrid
Madrid 28040, Spain

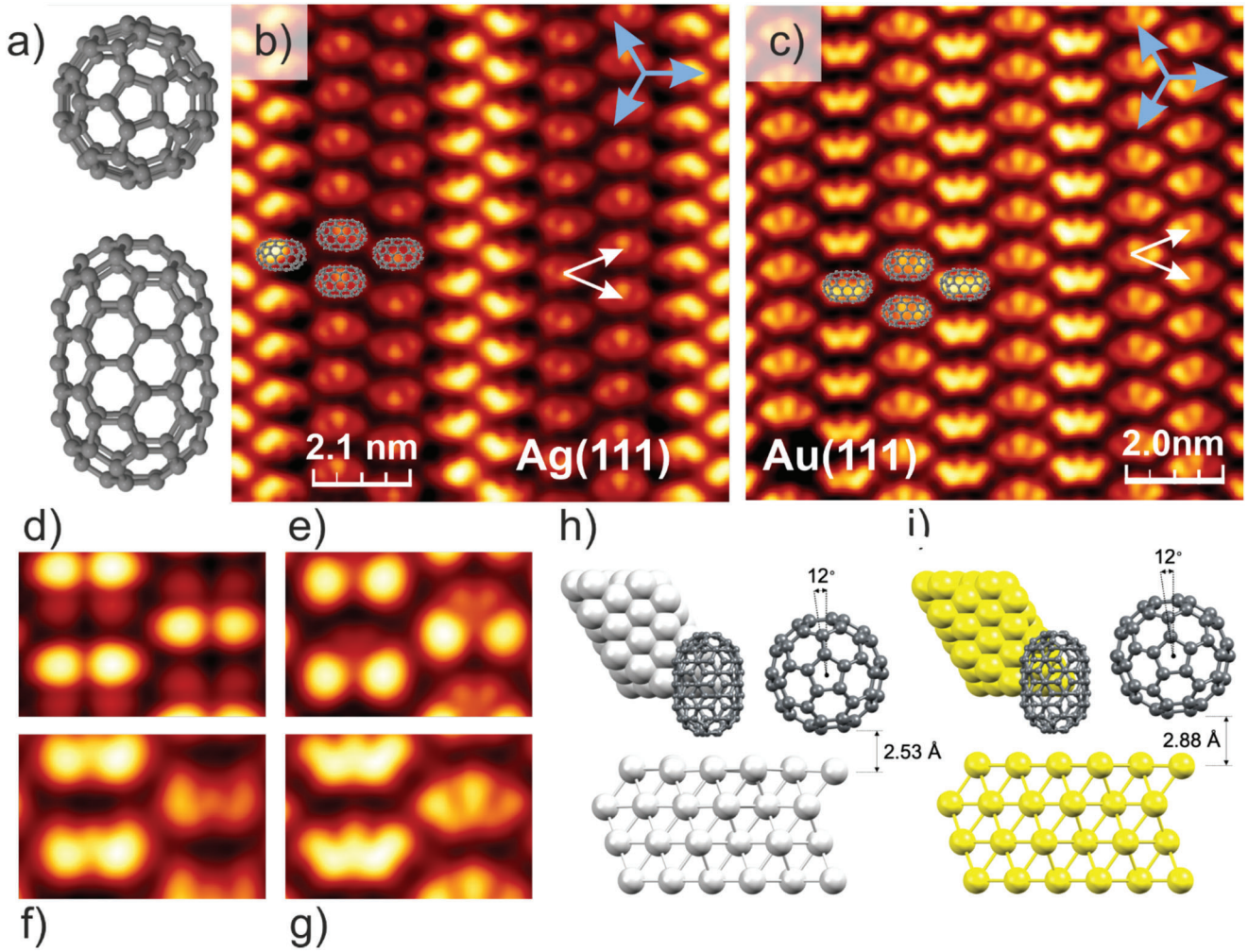

Figure 1. a) Stick-and-ball model of the [5,5] C_{90} (D_{5h}) fullertube used in these experiments. STM images of the adsorption of C_{90} molecules on b) Ag(111) and c) Au(111). The images were recorded with V_{bias} = 1.1 V and I_t = 1 nA (b) and V_{bias} = 1.7 V and I_t = 1.2 nA (c). White arrows represent the unit cell vectors of the molecular brick-wall structure, disregarding the orientational degree of freedom and registry with the substrate lattice. Blue arrows mark the close-packed directions of the underlying substrate. Experimental STM images recorded on Au(111) for different bias voltages: d) −1.35 V, e) 0.63 V, f) 1.10 V, and g) 1.7 V. The tunnel current setpoint for panels (d–g) is 1.2 nA. Panels (h) and (i) calculated adsorption equilibrium geometries for C_{90} fullertubes on Ag(111) and Au(111) surfaces, respectively.

fullertubes undergo a transition from more fullerene-like to more nanotube-like?

To shed light on these questions, in this paper, we have investigated the energies and wave-functions of the frontier orbitals of [5,5] C_{90}(D_{5h}) fullertubes (C_{90} in the following, see **Figure 1**a), adsorbed on Ag(111) and Au(111) surfaces, by means of low-temperature STM and STS, supported by density-functional theory (DFT) calculations. We show that HOMO and LUMO+2 orbitals present an electron density distribution that corresponds to that of the valence band in the associated infinite [5,5] CNT multiplied by a sinusoidal factor with one (HOMO) and two (LUMO+2) nodes. Moreover, a whole set of orbitals can be found with the same azimuthal dependence of the wave function, but 0, 1, 2, and 3 longitudinal nodes, demonstrating that they can be understood as the result of quantum confinement of the CNT valence band. Similarly, the electron density distribution of the LUMO orbital is compatible with a similar decomposition into the azimuthal dependence of the conduction band in [5,5] CNT times a sinusoidal factor with one node. On the contrary, the LUMO+1 orbital does not present the axial symmetry from the relevant bands around the Fermi level in [5,5] CNT. We are thus able to distinguish between nanotube-like and fullerene-like electronic states, as could be expected due to the hybrid nature of fullertubes. We believe that this classification is of the utmost importance for the understanding and categorization of fullertube properties, of the transition between CNT and fullerene molecules, and it might have significant implications for the development of applications ranging from solar cells to their use in molecular-electronic devices.

2. Results and Discussion

Figure 1 displays STM images of the adsorption and self-assembly of C_{90} on Ag(111) (b) and Au(111) (c). The molecular

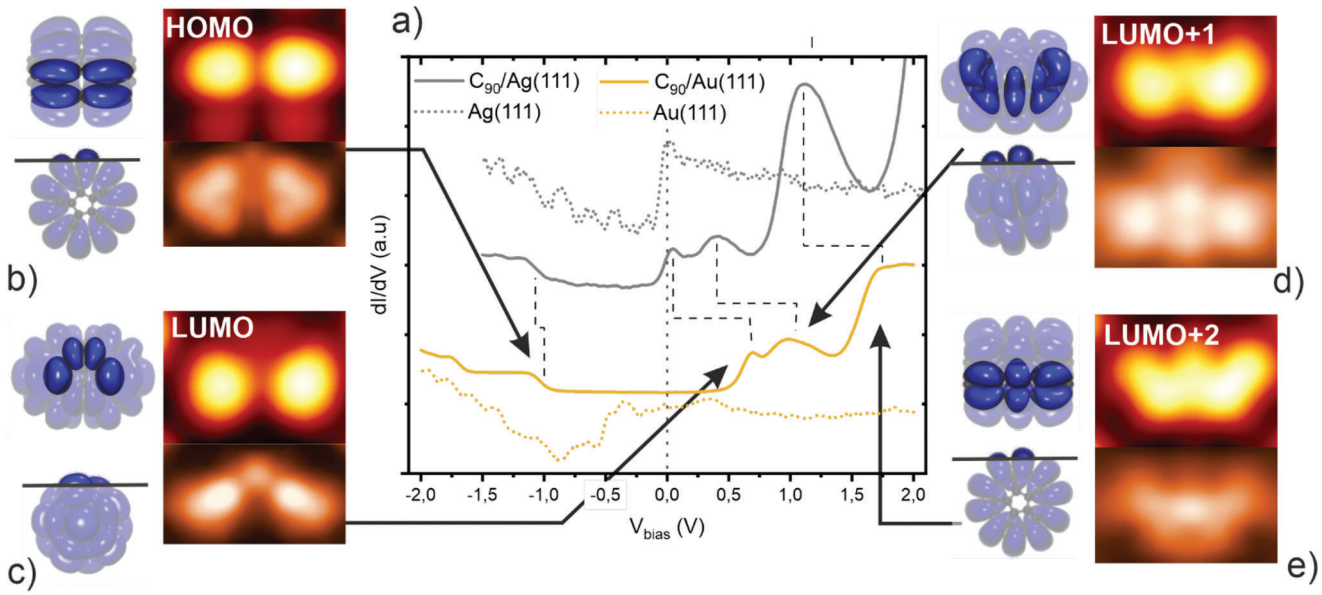

Figure 2. a) dI/dV curves recorded on C_{90} fullertube molecules adsorbed on Ag(111) and Au(111). Both curves show a similar spectral distribution, but with peaks positions that are shifted with respect to each other. Spectra obtained in clean areas of the surface are also shown, with clear features at the surface state energies. STM images corresponding to the voltages at which peaks are observed in (a) are shown in the top-right corner of panels (b–e). The images correspond well with the areas in which the calculated wave functions of HOMO, LUMO, LUMO+1, and LUMO+2 of isolated molecules (top- and side-views in the left sides of (b–e)) show the topmost lobes, taking into consideration the 12° axial orientation described in Figure 1. This correspondence is further supported by the calculated 2D maps of the wave-function modulus at a given height over the molecular axis (bottom-right corners in (b–e).

organization on both noble metal surfaces is very similar. Disregarding the molecular orientation and a larger-scale moiré like periodicity, the molecular lattice can be described as a brick-wall structure, with a rhombohedral unit cell of vectors $\mathbf{b}_1$ and $\mathbf{b}_2$ (see Figure 1) forming an angle of ≈45°. This implies an anisotropic distribution of intermolecular distances, being the molecules separated by ≈1.3 nm along the unit cell vectors, but only by ≈0.98 nm along the close-packed rows. Moreover, STM images individual molecules as elongated protrusions with a size of 1.4 × 0.8 nm (long axis × short axis), with the long axis directed along a close-packed direction of the underlying atomic lattice of the metallic surface. All these observations demonstrate a side-on adsorption of C_{90} molecules on the surface, similar to the adsorption geometry of CTNs on metal substrates.[13,14] This is also supported by our DFT calculations (see Figure 1h,i).

The brick-wall structure described above is very robust and can be found locally in very defective areas. However, in relatively large, defect-free areas (such as those shown in Figure 1b,c), new periodic structures can be identified: the ordering in the axial orientation of the molecules, and the appearance of a moiré-like alternation between bright and dark rows in the STM images. Such structures will be the subject of future works, but they do not affect in any significant way the electronic structure of the individual molecules (Section S5 and Figure S3, Supporting Information).

Interestingly, the binding of the C_{90} molecules to the surface seems to depend strongly on their axial orientation with respect to their long axis. In particular, our theoretical analysis has found several relaxed structures (Table S1, Supporting Information) with different axial angles, which we now characterize as the angle between the surface plane and that containing both the long axis of the molecule and the carbon–carbon bond from the upper pentagon in the capping fullerene (Figure 1h,i). Nonetheless, the energy minimum corresponding to the adsorption geometry with an axial angle of 12° turns out to be more stable than all the other ones by at least 0.1 eV. Inspection of the registry between the atomic arrangements of molecule and surface reveals that such an orientation allows to place the three lowermost carbon atoms of the C_{90} units on threefold hollow sites of the surface, enabling shorter molecule-surface distances and, thus, enhancing the binding energy.[15] As we will discuss below, this adsorption geometry seems to be the one obtained from our experiments, as evidenced by comparison between the experimental STM images and the theoretically calculated electron density maps.

It is also important to notice that the shape of the C_{90} molecules in the images is very strongly dependent on the applied bias voltage, revealing an important role of electronic structure factors on the STM images. This is exemplified in Figure 1d–g for the case of Au(111). We have further investigated the electronic structure of adsorbed C_{90} molecules by recording dI/dV curves. **Figure 2**a shows the average of 50 spectra recorded on a rectangular grid spanning the C_{90} molecule on Ag(111) (grey line) and Au(111) (yellow line). Location-dependent dI/dV curves are also shown in Figure S4 (Supporting Information), showing variations in the relative intensities of the different contributions, but not significant changes in the overall spectral shapes. The spectra measured on both surfaces reveal the HOMO as a conductance step ≈1 eV below the Fermi level. STM images simulated at the voltage corresponding to the theoretical energy of the HOMO level shows a good correspondence with the

experimental observations (Figure 2b, bottom-right panel). In particular, a transversal nodal line can be appreciated at the middle of the molecule. Also, a clear longitudinal node can be observed in the experimental images, which can also be faintly seen in the calculated images as a middle depression. These observations can be qualitatively rationalized by comparing to the calculated molecular orbitals of free-standing C_{90} molecules (see also Figure S5, Supporting Information). Taking into consideration the 12° axial angle described above, we can obtain a rough expectation for the STM images of this orbital simply by taking the topmost lobes of its wave function (non-shaded area in Figure 2b, left panel). This comparison allows us to identify the transversal and longitudinal nodal lines as arising from the HOMO orbital. The four protrusions observed in the experimental STM images correspond to the four uppermost lobes in the wave-function. The asymmetry between the lobes in the STM image with respect to the longitudinal nodal line arises from the 12° axial rotation of the C_{90} molecules.

For positive voltages (unoccupied energy levels), we find a series of three resonances, the first one relatively narrow, separated by 0.3 eV from the second resonance and ≈1 eV from the third resonance, both of which are significantly broader. The exact energies at which these resonances can be found, however, depend on the metal surface on top of which the C_{90} molecules are adsorbed, being 0.6 eV higher on Au(111) than on Ag(111), in good correspondence with the difference in their respective work functions (4.74 eV for Ag vs 5.31 for Au). The narrower electronic gap of C_{90} molecules on Ag(111) compared to Au(111) can be related to a decrease in the intermolecular electron–electron repulsion in the former, arising from the different electron transfer between the metal surface and the adsorbed molecule: whereas for Ag it amounts to ≈0.3 e^- from the metal to the molecule, for Au the transfer is from the molecule to the metal by ≈0.2 e^-, according to our theoretical calculations. Interestingly, however, our theoretical calculations predict something similar to a rigid shift of the electronic states when moving from Au(111) to Ag(111) (See Figure S6, Supporting Information), instead of the observed enlargement of the electronic gap with similar HOMO level energies in Figure 2a. A similar phenomenology has been reported for the comparison between experimental and theoretical data for C_{60} fullerene on Ag and Au surfaces[16,17] which was attributed to different screening of the intramolecular repulsion energy due to the different charge transfer from the metal to the molecule.

Like we did for the HOMO, we can also compare the STM images obtained at the voltages that correspond to the unoccupied resonances, with the calculated shapes of the LUMO, LUMO+1, and LUMO+2 orbitals, finding again a noticeable resemblance. Moreover, the three-lobe appearance of C_{90} molecules in our STM images can now be traced to the existence of two transversal nodal lines in the wave-function instead of just one, a fact that will become significant later. We thus conclude that the shapes of the orbitals found in the theoretical calculations are supported by our experiments.

At this point, it is interesting to compare the spatial extension of such frontier orbitals in C_{90} with the delocalized (Bloch) states that are characteristic of the infinite [5,5]-SWCNT. Since the delocalized electronic states in the nanotube are described by Bloch wave function $e^{ikx}u(\mathbf{r})$, the spatial extension of the electronic states at the Γ point ($k = 0$) can be understood as a plot of $u(\mathbf{r})$, and any other wave function corresponding to a non-vanishing value of k within the same band is simply the product of $u(\mathbf{r})$ by a 1D harmonic wave. Calculated density maps for these bands are shown to the right in **Figure 3**, corresponding nicely with previous experimental observations for nanotubes on metal surfaces.[13,14] If the nanotube had a finite length L, quantum confinement would discretize the allowed values for the electron's momentum as $k_n = n\pi/L$ where, n is an integer number, and the wave-function of such an electronic state would be given by the product of $u(\mathbf{r})$ times a sinusoidal standing wave with $n - 1$ nodes. Comparison between the wave functions of the fullertubes HOMO and LUMO+2 orbitals with the nanotube wave function for the Valence Band in Figure 3a,b shows that, indeed, these orbitals can be understood as the result of the quantum confinement of the electrons in the valence band of the infinite nanotube to the length of the fullertube with $n = 2$ and $n = 3$, respectively. The molecular orbitals present nodes at both hemifullerene terminals, have the same distribution with the azimuthal angle around the nanotube, and present one (HOMO) or two (LUMO+2) transversal nodal lines. Similarly, our theoretical calculations predict two more orbitals with the same azimuthal dependence of the wave function and 0 or 3 longitudinal nodes (see Figure S7, Supporting Information). Moreover, similar states can also be found in the theoretical calculations corresponding to larger fullertubes, such as C_{100} and C_{120}. In all these cases, the energies of such orbitals scale quadratically with the number of nodes, and, for the same number of nodes, decrease with the fullerene length (see Figure S7, Supporting Information), all of which suggest that they originate from quantum confined band states of the infinite nanotube.

The strong confinement at the fullerene endcaps leads to a marked node at these positions. This could be forced by symmetry reasons: the valence band wave functions are characterized by zig–zag lobes running along the carbon–carbon chains parallel to the molecular axis, with alternating signs in the azimuthal direction. At the fullerene endcaps, however, this carbon–carbon chains merge into the end pentagons and, thus, these orbitals could not possibly extend to the fullerene terminals.

The LUMO orbital, on the other hand, exhibits the same distribution with the azimuthal angle than the Conduction Band of the [5,5]-SWCNT (Figure 3b) and has a transversal nodal line at the middle of the molecule, suggesting that it might also arise from the quantum confinement of this band. However, this orbital does not show nodes at the hemifullerene moieties, which indicates mixing between these confined states and fullerene-like orbitals localized at the terminals. Notice that the wave functions of the [5,5] CNT conduction bands show elongated lobes linking neighboring atoms in the perpendicular direction to the molecular axis, and this pattern is not incompatible with the fullerene cap structure.

Finally, the LUMO+1 orbital presents a dependence with the polar angle that is incompatible with any of the SWCNT bands, since its wave function lacks the fivefold axial symmetry that characterizes the [5,5]-CNT band structure (see Figure S5, Supporting Information, for a complete description of the calculated molecular orbitals). The LUMO+1 orbital also has a rather large weight of the wave function at the hemifullerene terminals (see Figure 2d), indicating that this electronic state is fullerene-like in character, with little relation to the delocalized electronic states of

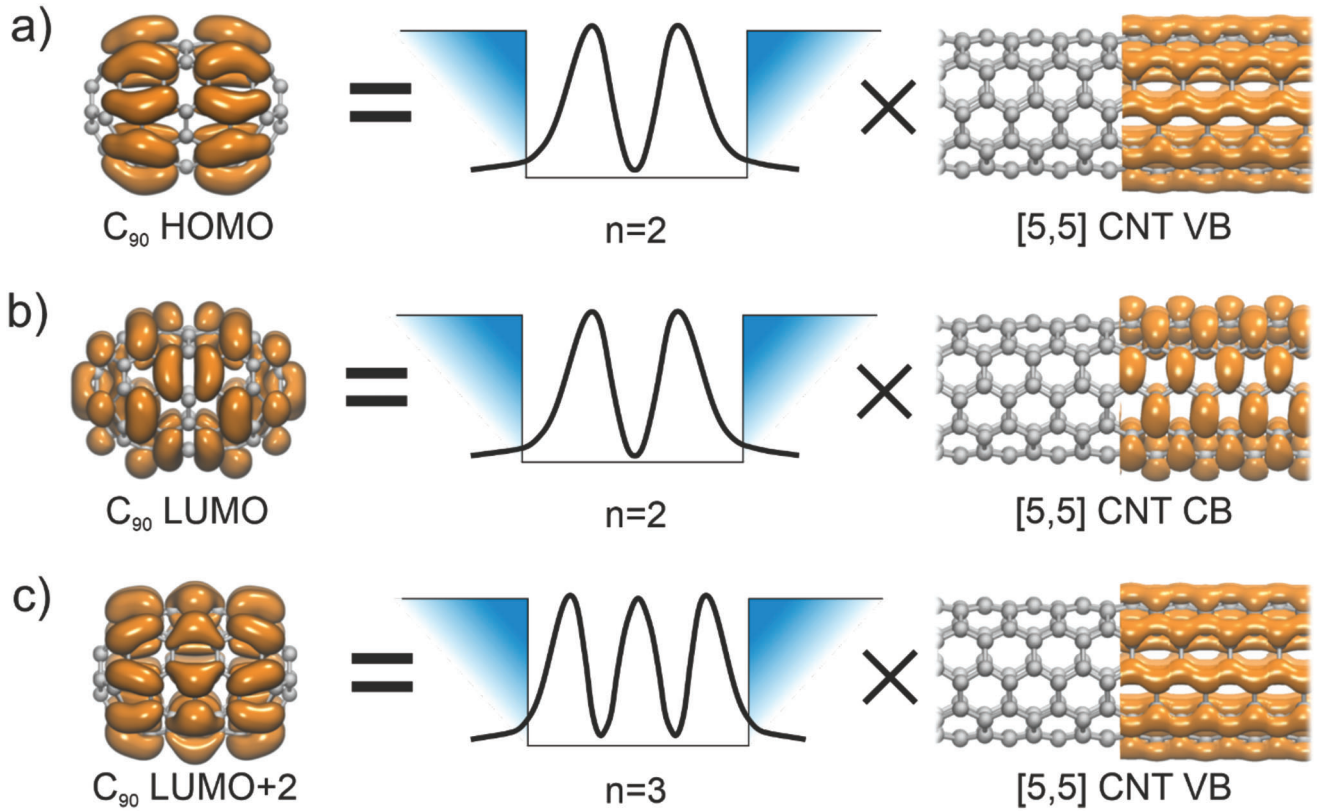

Figure 3. Decomposition of the C90 fullertube HOMO (a), LUMO (b), and LUMO+2 (c) orbitals into a factor that contains information about the wave function of the associated [5,5] infinite SWCNT, and a sinusoidal factor arising from the confinement of the delocalized band states to the finite size of the molecular backbone.

the nanotube. We thus have found that some molecular orbitals of C_{90} can be regarded as arising from the quantum confinement of [5,5]-CNT, since the polar dependence of wave-functions of the former match the polar dependence of the delocalized Bloch states of the latter. We call these states "nanotube"-like. On the other hand, other orbitals present a different axial symmetry which is incompatible with that of the CNTs, and can thus be considered as "fullerene"-like.

3. Conclusion

To conclude, we have investigated the electronic states of fullertubes deposited on compact noble-metal surfaces by means of scanning tunneling microscopy and density functional theory calculations. The molecular orbitals estimated from the bias dependence of the STM images at the corresponding STS resonances correspond quite closely to those expected from gas-phase calculations. This combined experimental and theoretical effort has allowed us to propose a classification of the electronic states of fullertubes depending on their resemblance to the electronic states in infinite [5,5]-SWCNT: while some orbitals can be considered as "nanotube"-like, since they arise from quantum confinement of the delocalized Bloch states in the infinite nanotube, some others cannot be understood in this way due to their axial symmetry, and thus they can be considered as purely fullerene-like in character. We believe that this new insight is essential for the understanding of the hybrid nature of emergent fullertubes as well as for the optimization of their properties for future applications.

Supporting Information

Supporting Information is available from the Wiley Online Library or from the author.

Acknowledgements

O.J. and A.M.-J. contributed equally to this work. R.M. and R.O. acknowledge financial support from the Spanish Ministry for Science and Innovation (Grants PID2020-113142RB-C21, PLEC2021-007906, and PID2021-128011NB-I00), and N.M. to the Project PID2020-114653RB-I00). the regional government of Comunidad de Madrid (Grant S2018/NMT-4321, S2018/NMT-4367, and Y2020/NMT6469), Universidad Autónoma de Madrid (UAM/48) and IMDEA Nanoscience. Both IMDEA Nanoscience and IFIMAC acknowledge support from the Severo Ochoa and Maria de Maeztu Programmes for Centres and Units of Excellence in R&D (MICINN, Grants CEX2020-001039-S and CEX2018-000805-M). R.O. acknowledges support from the excellence program for University Professors, funded by the regional government of Madrid (V PRICIT). SS acknowledges support from NSF through grant # CHE-1856461. The authors acknowledge the support from the "(MAD2D-CM)-UAM" project funded by Comunidad de Madrid, by the Recovery, Transformation and Resilience Plan, and by NextGenerationEU from the European Union.

Conflict of Interest

The authors declare no conflict of interest.

Data Availability Statement

The data that support the findings of this study are available from the corresponding author upon reasonable request.

Keywords

adsorption, carbon nanoforms, carbon nanotubes, electronic structures, higher fullerenes

Received: October 5, 2023
Published online: October 20, 2023

[1] S. Stevenson, X. Liu, D. M. Sublett, R. M. Koenig, T. L. Seeler, K. R. Tepper, H. M. Franklin, X. Wang, R. Huang, X. Feng, K. Cover, D. Troya, N. Shanaiah, R. J. Bodnar, H. C. Dorn, *J. Am. Chem. Soc.* **2021**, *143*, 4593.
[2] X. Liu, E. Bourret, C. A. Noble, K. Cover, R. M. Koenig, R. Huang, H. M. Franklin, X. Feng, R. J. Bodnar, F. Zhang, C. Tao, D. M. Sublett, H. C. Dorn, S. Stevenson, *J. Am. Chem. Soc.* **2022**, *144*, 16287.
[3] R. M. Koenig, H.-R. Tian, T. L. Seeler, K. R. Tepper, H. M. Franklin, Z.-C. Chen, S.-Y. Xie, S. Stevenson, *J. Am. Chem. Soc.* **2020**, *142*, 15614.
[4] D. C. Agrawal, *Introduction to Nanoscience and Nanomaterials*, World Scientific, Singapore **2013**, pp, 237–279.
[5] C. T. White, T. N. Todorov, *Nature* **1998**, *393*, 240.
[6] J. L. Delgado, M. Herranz, N. Martín, *J. Mater. Chem.* **2008**, *18*, 1417.
[7] N. Martín, *Adv. Energy Mater.* **2017**, *7*, 1601102.
[8] R. Otero, D. Écija, G. Fernández, J. M. Gallego, L. Sánchez, N. Martín, R. Miranda, *Nano Lett.* **2007**, *7*, 2602.
[9] L. Sánchez, R. Otero, J. M. Gallego, R. Miranda, N. Martín, *Chem. Rev.* **2009**, *109*, 2081.
[10] K. S. Novoselov, A. K. Geim, S. V. Morozov, D. Jiang, M. I. Katsnelson, I. V. Grigorieva, S. V. Dubonos, A. A. Firsov, *Nature* **2005**, *438*, 197.
[11] S. Mishra, D. Beyer, R. Berger, J. Liu, O. Gröning, J. I. Urgel, K. Müllen, P. Ruffieux, X. Feng, R. Fasel, *J. Am. Chem. Soc.* **2020**, *142*, 1147.
[12] S. Mishra, D. Beyer, K. Eimre, S. Kezilebieke, R. Berger, O. Gröning, C. A. Pignedoli, K. Müllen, P. Liljeroth, P. Ruffieux, X. Feng, R. Fasel, *Nat. Nano.* **2019**, *15*, 22.
[13] H. Lin, J. Lagoute, V. Repain, C. Chacon, Y. Girard, F. Ducastelle, H. Amara, A. Loiseau, P. Hermet, L. Henrard, S. Rousset, *Phys. Rev. B* **2010**, *81*, 235412.
[14] S. G. Lemay, J. W. Janssen, M. van den Hout, M. Mooij, M. J. Bronikowski, P. A. Willis, R. E. Smalley, L. P. Kouwenhoven, C. Dekker, *Nature* **2001**, *412*, 617.
[15] J. D. Martin, J. N. Marhefka, K. B. Migler, S. D. Hudson, *Adv. Mater.* **2011**, *23*, 426.
[16] X. Lu, M. Grobis, K. H. Khoo, S. G. Louie, M. F. Crommie, *Phys. Rev. B* **2004**, *70*, 115418.
[17] I. Fernández Torrente, K. J. Franke, J. Ignacio Pascual, *J. Phys. Cond. Mat.* **2008**, *20*, 184001.